

Analyst

Accepted Manuscript



This is an *Accepted Manuscript*, which has been through the Royal Society of Chemistry peer review process and has been accepted for publication.

Accepted Manuscripts are published online shortly after acceptance, before technical editing, formatting and proof reading. Using this free service, authors can make their results available to the community, in citable form, before we publish the edited article. We will replace this *Accepted Manuscript* with the edited and formatted *Advance Article* as soon as it is available.

You can find more information about *Accepted Manuscripts* in the [Information for Authors](#).

Please note that technical editing may introduce minor changes to the text and/or graphics, which may alter content. The journal's standard [Terms & Conditions](#) and the [Ethical guidelines](#) still apply. In no event shall the Royal Society of Chemistry be held responsible for any errors or omissions in this *Accepted Manuscript* or any consequences arising from the use of any information it contains.

Analysis of fast channel blockage: revealing substrate binding in the microsecond range[†]

Igor Bodrenko,^a Harsha Bajaj,^b Paolo Ruggerone,^a Mathias Winterhalter,^b and Matteo Ceccarelli^{*a}

Received Xth XXXXXXXXXXXX 20XX, Accepted Xth XXXXXXXXXXXX 20XX

First published on the web Xth XXXXXXXXXXXX 200X

DOI: 10.1039/b000000x

For an antibiotic to be effective, it needs to cross the outer membrane barrier and to reach target inside the cell. Hydrophilic antibiotics, e.g. β -lactams, use porin channels to cross the outer membrane and accumulate in the periplasm. Experimental determination of antibiotic interaction with porin is performed by using electrophysiology on a single channel level by noise analysis or single event analysis methods. We report a novel framework for analyzing the ion-current noise, taking into account the corrections due to the analogous filter and the sampling procedure, with the goal to extend the time resolution into the range previously inaccessible by event analysis or by conventional noise analysis. The new method allows one to analyse fast binding events and/or the cases when the single channel is not completely blocked by the substrate. We demonstrate the power of this approach by using the example of meropenem, an antibiotic of the carbapenem family, interacting with the OmpF porin which is considered to be one of the main pathways for antibiotics to enter *Escherichia coli*. The presence of meropenem in OmpF is detected by ion current blockages, and the *on* and *off* rates are obtained from the concentration dependence of the average ion current and of its power spectral density. The obtained average residence time of the antibiotic inside the channel is in the range of few microseconds, i.e. more than 50 times smaller than the inverse cutoff frequency of the analogous filter.

1 Introduction

The complex membrane of Gram-negative bacteria controls the selective passage of nutrients and waste into and from the cell cytoplasm. Influx of solute is largely restricted by porins, which are water-filled open channels that span the outer membrane of Gram-negative bacteria and allow the passive penetration of hydrophilic molecules^{1,2}. Apart from various nutrient molecules, many classes of antibiotics like β -lactams are also known to use outer membrane channels to reach their target inside the cell². Consequently, bacterial adaptation to reduce influx through porins is an increasing problem worldwide that contributes, together with efflux or/and enzymatic systems, to the emergence and dissemination of antibiotic resistance^{1,3,4}. This highlights the need to measure antibiotic translocation rate through porin in a quantitative manner to rationalize the permeation mechanism through porins and identify new potential antibacterials.

An appropriate method to analyze the physico-chemical properties of these porins, like conductance, selectivity and voltage gating, is reconstitution of porins in planar lipid bilayer and measuring an ion current through the lipid bilayer^{5,6}.

[†] Electronic Supplementary Information (ESI) available: Computational procedure and data analysis protocol. See DOI: 10.1039/b000000x/

^a Department of Physics, University of Cagliari, S.P. Monserrato-Sestu km 0.700, I-09042 Monserrato (CA), Italy. Fax: +39-070-6753191; Tel: +39-070-6754933; E-mail: matteo.ceccarelli@dsf.unica.it

^b Jacobs University, Campus Ring 1, 28759 Bremen, Germany.

Interaction between substrates (sugars, antibiotic, peptides) and outer membrane channel has been characterized using planar lipid technique in a quantitative manner^{5,7-9}. For example, the binding constant of sugars through LamB channel (sugar specific channel), explained by a simple two-barrier one-binding-site model, has been probed using pore conductance^{5,10}. An analysis of the conductance with respect to the sugar concentration yields information about the affinity constant K of the sugar to the channel lumen⁵.

To address transport of sugars through maltoporin, Benz and his colleagues had initiated noise analysis of ion currents through reconstituted maltoporin channels¹¹. In contrast to the binding constants, that are determined from the effect of sugar addition on the average current, the noise analysis gives the absolute rates of the sugar binding reaction. Results of spectral analysis of sugar-induced noise in current were well fitted by Lorentzian power spectral densities^{11,12}. Lorentzian spectra are usually associated with two-state Markovian processes; therefore the binding process can be approximated by such a process, where one state being a pore occupied by a sugar molecule and the other state corresponding to an empty pore. The corner frequency values, obtained by fitting the experimental ion-current power spectra to Lorentzian at different sugar concentrations, was used to calculate the k_{on} (association) and k_{off} (dissociation) rates of the maltose sugars (maltotriose to maltopheptaose) in LamB channel¹¹.

Experimental studies of sugar-LamB interaction were at-

tempted at single channel level, where the authors observed time resolved ion current fluctuations¹³ in presence of sugars unlike a reduction in conductance observed in multichannel system¹². One of the advantages to work with a single channel is that the individual kinetic rates constants can be obtained directly by single event analysis of ion current inhibitions caused by substrate residing in the channel⁷. For example OmpF, the outer membrane protein F from *Escherichia coli* involved in the uptake of antibiotics, was characterized in presence of several β -lactams at a single channel level in planar lipid bilayer¹⁴. Transient downward current steps with the amplitude of one-third (monomer) of the total initial current through the channel correspond to time-resolved events of antibiotic binding to channel^{7,14}. These events are reversible and each of them is caused by a single antibiotic molecule entering the aqueous pore of one subunit of the OmpF trimer. The average time between successive blockages is observed to decrease with increasing antibiotic concentration and provides the association rate constant⁷. The dissociation rate on the other hand is the inverse of residence time of the antibiotic in the channel, which is determined experimentally from the dwell time histogram analysis of events⁷. Inspection of ion current fluctuation through the porin at a single channel level in presence of antibiotics provides comparable thermodynamic and kinetic parameters both in single event method/noise analysis method^{7,14,15}.

These methods suffer from the time resolution problem: blockage faster than 50 μ s cannot be well resolved¹⁶. Several experimental techniques were proposed to study the fast blockages. Thus, the kinetics can be slowed down by decreasing the temperature¹⁷ or by adding ionic liquid¹⁸. In this context, we should also mention a different technique, the so-called liposome swelling method¹⁹, which provide complementary information on the permeation.

In the present paper, we demonstrate how to improve the time resolution by using an advanced noise analysis. In particular, we investigated the interaction of meropenem, a β -lactam antibiotic, with single trimeric OmpF channel in planar lipid bilayer. Addition of meropenem into the solution causes an increase in the ion-current noise and subsequent decrease in the average conductance of pore in planar lipid bilayer experiments. However, single events are too fast to be resolved using the conventional noise analysis. We calculated the auto-correlation function of the ion current trace and then, after the Fourier transformation, we obtained the power spectral density. The power spectrum was fitted with a Lorentzian function taking into account the sampling and the filter correction factors. As expected, the power spectral density and the average ion current depend on the antibiotic concentration and, thus, allow one to obtain the kinetic parameters from the concentration dependence. The equilibrium constant ($K = k_{\text{on}}/k_{\text{off}}$) calculated from the rates obtained in our analysis including

the correction factors agreed well with that obtained by the equilibrium titration using the averaged ion conductance.

The analysis of the data for meropenem supports the idea that accounting for correction factors has a potential to reveal the fast events, increasing the power of the single channel technique as a tool for a more reliable characterization of substrates translocation through porins. Information extracted from experiments and analyzed according to the procedure described here might be converted into data related to the interaction of compounds with the porins and, thus, provide insights possibly useful to rationalize drug design.

2 Theory

The effect of a substrate onto the ion current through a membrane channel results in a shift of the average current (reduction of the conductance) and in an increase of the current fluctuations (see Figure 1).

If the average current through a single open monomer channel is j_0 and that through the monomer channel occupied by a substrate is j_1 then, within the two-state Markov model, the average current through the multimer pore reads

$$j_{\text{av}}(c) = N_c [j_1 P(c) + j_0 (1 - P(c))] \quad , \quad (1)$$

where N_c is the number of the monomer channels in the multimer pore and $P(c)$ is the equilibrium probability to find a monomer channel occupied by a substrate at concentration c of the latter. At zero concentration, the probability to find a substrate molecule in a channel is zero, and one has, $j_{\text{av}}(0) = j_0 N_c$. Then, by expressing the occupation probability, $P(c)$, in terms of the transition rates^{11,20}, one obtains the shift of the average current through the channel due to the presence of the antibiotic,

$$\langle \Delta j \rangle = |j_{\text{av}}(c) - j_{\text{av}}(0)| = \frac{N_c \Delta j c k_{\text{on}}}{k_{\text{off}} + c k_{\text{on}}} \quad , \quad (2)$$

where $\Delta j = |j_1 - j_0|$ is the absolute difference of the average current in the open monomer channel and that in the blocked one at the given applied potential; k_{off} and k_{on} are the dissociation and the association rates, respectively. If the channel is completely blocked by the substrate, then $\Delta j = |j_{\text{av}}(0)|/N_c = j_0$,^{11,20}. If the ion current through the channel occupied by a substrate molecule is not completely blocked then $\Delta j < |j_0|$.

The power spectral density (PSD) of the ion current fluctuations due to the blockages by the antibiotic molecules in the two-state Markov model reads⁷,

$$G(f) = \frac{a}{1 + (2\pi f \tau_c)^2} \quad ; \quad (3)$$

$$a = 4N_c (\Delta j)^2 c k_{\text{on}} k_{\text{off}} \tau_c^3 \quad ; \quad (4)$$

$$\tau_c = \frac{1}{k_{\text{off}} + c k_{\text{on}}} \quad . \quad (5)$$

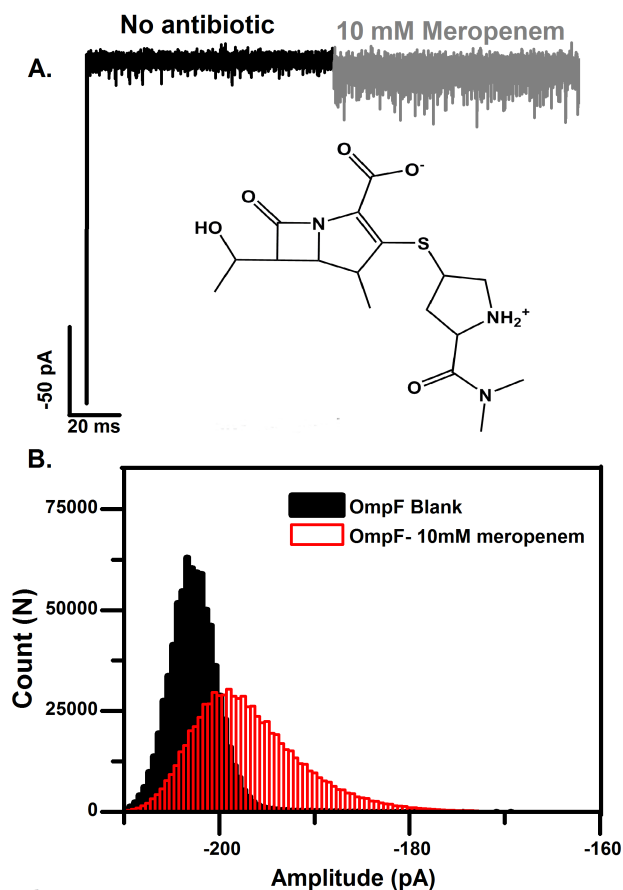


Fig. 1 A. Ion current trace of single OmpF channel in presence and absence of 10 mM Meropenem (chemical structure is shown in the panel). B. Corresponding histogram of ion current (10 seconds of trace) through OmpF in absence (black) and presence of 10mM Meropenem (red). Conditions: 1M KCl, 20 mM MES pH 6 at -50 mV.

Here, τ_c indicates the correlation time of the blockage process.

In case $k_{\text{off}} \gg ck_{\text{on}}$, the average current shift, $\langle \Delta j \rangle$, as well as the Lorentzian factor, a , of the PSD may be expanded up to the second order in concentration as:

$$\langle \Delta j \rangle (c) = N_c \Delta j \frac{ck_{\text{on}}}{k_{\text{off}}} \left(1 - \frac{ck_{\text{on}}}{k_{\text{off}}} \right) + o \left(\left(\frac{ck_{\text{on}}}{k_{\text{off}}} \right)^2 \right) ; \quad (6)$$

$$a(c) = \frac{4N_c (\Delta j)^2}{k_{\text{off}}} \frac{ck_{\text{on}}}{k_{\text{off}}} \left(1 - 3 \frac{ck_{\text{on}}}{k_{\text{off}}} \right) + o \left(\left(\frac{ck_{\text{on}}}{k_{\text{off}}} \right)^2 \right) . \quad (7)$$

In the electrophysiology experiments, the ion-current signal is filtered by an analogous low-pass linear filter and then sampled at a specific rate, $f_s = 1/\Delta t$. The sampling procedure consists of the averaging of a signal for the period Δt

and, thus, corresponds to the application of a linear filter after the first analogous one. The average value of the ion-current signal, j_{av} , is not affected by a linear filter whereas the dispersion, the auto-correlation function, and the PSD are modified by both filters. If the transfer function of the analogous filter is $H_a(\omega)$ and that of the sampling filter is $H_s(\omega)$, then the relation between the PSD of the original ion current, Eq. (3), and that of the signal after successive application of the two filters is the following²¹

$$G_m(f) = \frac{a}{1 + (2\pi f \tau_c)^2} |H_a(2\pi f)|^2 |H_s(2\pi f)|^2 . \quad (8)$$

At small frequencies, $f \approx 0$, the transfer functions are close to 1 and do not modify the PSD. At large frequencies, $f \gg f_c$ (f_c is the filter cutoff frequency) or $f \gg 1/\Delta t$, the original PSD is suppressed by the filters. Thus, if the correlation time, τ_c , of the ion-current signal which determines the width of the PSD [see, e.g., Eq. (3)] is close to or smaller than the sampling interval Δt or f_c^{-1} then filters corrections are very important for the PSD analysis.

By fitting the PSD of the observed signal to the filters-corrected Lorentzian model [Eq. (8)], one can obtain a and τ_c at different concentration of the substrate. The computational procedure and the data analysis protocol are described in details in the *Electronic Supplementary Information*.

Once model parameter a is determined, then depending on the availability of τ_c and of $\langle \Delta j \rangle$, one may use the alternative approaches outlined below to extract the kinetic parameters, k_{off} and k_{on} , characterizing the substrate-channel interaction.

Method 1. If the correlation time, τ_c , and the Lorentzian factor, a , are determined by fitting the experimental PSD to form (8), and Δj is known, e.g. from the ion-current frequency histogram, then the kinetic parameters can be calculated from Eqs. (4) and (5) (assuming $k_{\text{off}} > ck_{\text{on}}$),

$$k_{\text{off}} = \frac{1}{2\tau_c} \left(1 + \sqrt{1 - \frac{a}{N_c \tau_c (\Delta j)^2}} \right) ; \quad (9)$$

$$k_{\text{on}} = \frac{1}{2\tau_c c} \left(1 - \sqrt{1 - \frac{a}{N_c \tau_c (\Delta j)^2}} \right) . \quad (10)$$

Method 2. If Δj is unknown *a priori*, one can still determine k_{off} and k_{on} from the concentration dependence of the correlation time by using Eq. (5). Then, Δj may be also calculated from (4) as follows,

$$\Delta j = \sqrt{\frac{a}{4N_c ck_{\text{on}} k_{\text{off}} \tau_c^3}} . \quad (11)$$

Method 3. If the correlation time is very small and it is not possible to determine it by fitting Eq. (8) to the experimental PSD, one may utilize the antibiotic concentration dependence measurements and fit the Lorentzian factor, a , and the average

current shift, $\langle \Delta j \rangle$, by using the following equations, respectively:

$$a(c) = b_a c (1 - 3rc); \quad (12)$$

$$\langle \Delta j \rangle (c) = b_j c (1 - rc), \quad (13)$$

where the fitting parameter $r = K = k_{\text{on}}/k_{\text{off}}$ is equals to the equilibrium (or stability) constant of the antibiotic-channel interaction. Then, by using Eqs. (6) and (7), one obtains,

$$k_{\text{on}} = \frac{4b_j^2}{N_c b_a}; \quad (14)$$

$$k_{\text{off}} = \frac{k_{\text{on}}}{r}; \quad (15)$$

$$\Delta j = \frac{b_j}{N_c r}. \quad (16)$$

Method 4. If the correlation time is very small and its dependence on antibiotic concentration is not accessible but an *a priori* knowledge of Δj is possible, then one can determine the kinetic parameters from the concentration dependence of the PSD Lorentzian factor, $a(c)$, and of the average current shift, $\langle \Delta j \rangle$. In this case, one fits first the function

$$\langle \Delta j \rangle (c) = N_c \Delta j (1 - rc)rc \quad (17)$$

to the experimental average current shift and determines the equilibrium constant $K = r$. This step is similar to the conductance probe method⁵ except for the fact that we use the second-order expansion in the latter equation instead of the exact formula given by Eq. (2) used in⁵. In the second step, by fitting Eq. (12) to the concentration dependence of the Lorentzian factor keeping r fixed, one determines parameter b_a and then obtains,

$$k_{\text{off}} = \frac{4N_c (\Delta j)^2 r}{b_a}; \quad (18)$$

$$k_{\text{on}} = r k_{\text{off}}. \quad (19)$$

3 Experiment – Single channel electrophysiology

To form planar lipid bilayer with the lipid monolayer opposition technique²² we used a 5 mg/mL solution of 1,2-diphytanoyl-sn-glycero-3-phosphocholine (Avanti Polar Lipids, Inc., Alabaster, AL) in pentane. Bilayer is formed across a 50- 100 μm diameter aperture in 25 μm thick Teflon partition. Silver chloride electrodes from WPI (World Precision Instruments), one connected to the live side of amplifier (referred to as trans side; where the voltage is applied) and other connected to the ground side (referred to as cis side) are used. Small amount (upto 0.1 μL) of wild-type OmpF from a diluted stock solution of 60 ng/mL in 1% (v/v) of genapol

Table 1 Specification of the independent measurements for OmpF/meropenem. Columns from left to right: the number of the data set, used concentrations of the substrate, used sampling rates.

set	c , mM	f_s , kHz
1	0, 2.5, 5, 7.5, 9	50
2	0, 2.5, 5, 7.5, 10	50
3	0, 5, 10, 12.5, 15, 20, 23	50, 250
4	0, 5, 10, 12.5, 15, 20, 24	50, 250
5	0, 5, 10, 12.5, 15, 20, 24	50, 250

is added to the cis side of the chamber. Spontaneous insertion of single OmpF channel usually happens within minutes after protein addition to the aqueous phase with volume of 250 μL (1 M KCl, 20 mM MES, and pH 6). Both the small-ion conductance and the gating properties are used as an indication for directional channel insertion (likely with cis side of the lipid bilayer corresponds to the extracellular side of the porin 80% of times). Our convention is plus sign (positive voltage) means the trans side of the membrane cell compartment is more positive. Conductance measurements were performed using an Axopatch 200B amplifier (Axon Instruments, Inc., Foster City, CA) in the voltage clamp mode. Data were filtered by a low-pass 4-pole Bessel filter at 10 kHz with a sampling frequency of 50 kHz or 250 kHz and recorded simultaneously into the computer memory. Meropenem (Sequoia research products) stock solutions were made up to 40 mM in 1 M KCl, 20 mM MES pH 6 and added in a concentration dependent manner to the cis side of the chamber and diluted at the end of measurements for blank pore/control measurements. Chemical structure of meropenem (MW 383 g/mol) is shown in Fig.1A; the molecule is zwitterionic at the conditions of measurements. Due to the heating of the amplifier, many times we observed increase of temperature (up to 2-3 $^{\circ}\text{C}$ increase from room temperature) in the cuvette of small volumes (250 μL). For this reason the measurements were finished within 2 - 3 hours to minimize (although not completely eliminate; increase to 1-1.5 $^{\circ}\text{C}$ observed) conductance/transport properties fluctuation due to temperature changes.

We performed several independent electrophysiology measurements. The specifications of the measurements are collected in Table 1.

4 Results

In the presents investigation, we studied meropenem interaction with OmpF. Addition of meropenem to a single trimeric OmpF channel caused unresolved short flickering and subsequent reduction in ion current (Figure 1A).

According to the proposed data analysis protocol described in *Electronic Supplementary Information*, for each measure-

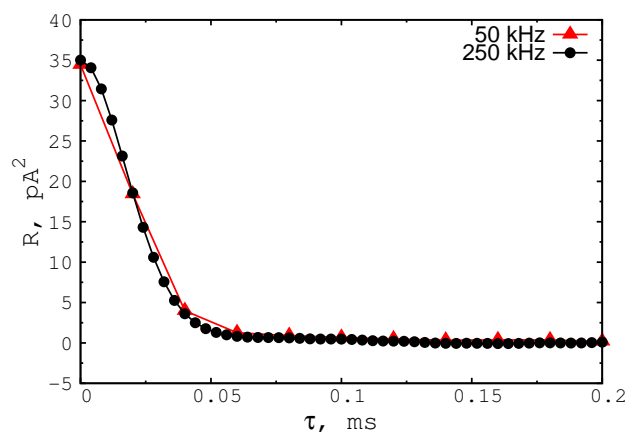


Fig. 2 Auto-correlation function of the ion current fluctuations sampled at 50 kHz rate (red triangles) and at 250 kHz rate (black circles). Data set 3, see Tab.1, $c = 10$ mM.

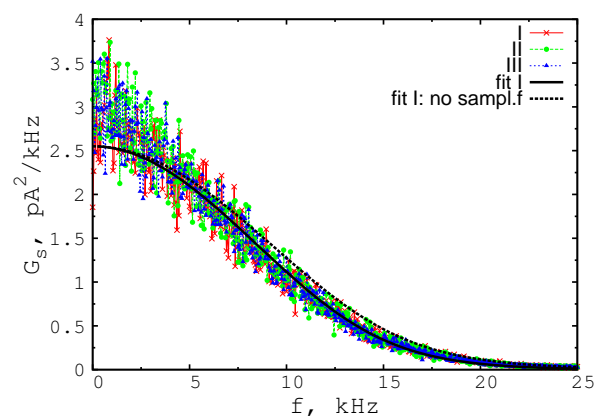
ment specified in Table 1 (at each concentration of the substrate), we selected 3 independent data records, denoted below by *I*, *II* and *III*. The duration T of the records equals 5 seconds for the data sampled at 50 kHz rate (2.5×10^5 events) and 4 seconds for the data sampled at 250 kHz rate (10^6 events).

The ion-current event frequency histograms do not have the secondary peak but exhibit a strong asymmetry (Figure 1B). Thus, it is impossible to determine Δj directly. There is no evidence of the spontaneous channel gating at present conditions.

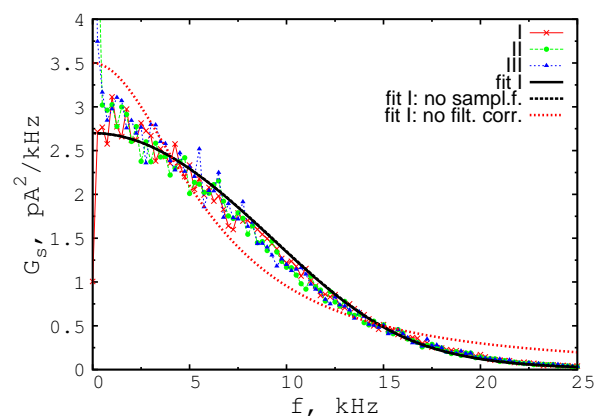
The auto-correlation function, $R(\tau)$, is calculated for τ up to $\tau_{\max} = 20$ ms for the data sampled at 50 kHz rate and up to $\tau_{\max} = 4$ ms for the data sampled at 250 kHz rate. As an example, the auto-correlation functions of the ion current sampled at 50 kHz and that sampled at 250 kHz are shown in Figure 2 for a small range of τ to show the significant details.

For all data sets, the signal PSD, $G_s(f)$, calculated according to Eq. (20) of the *Electronic Supplementary Information* by subtracting the background PSD, is well fitted by the filters-corrected Lorentzian, Eq. (8). However, the fitting procedure allows one to determine only the upper bound of the correlation time, i.e., it could be only stated that $\tau_c < 0.01$ ms in the case of the 50 kHz sampling and $\tau_c < 0.005$ ms for the 250 kHz sampling. The signal PSD of the ion current sampled at 50 kHz and that sampled at 250 kHz are shown in Figure 3 (panel A and B, respectively) for the three data records (the ion-current data are taken from set 3, see Tab.1, for $c = 10$ mM; the PSDs for data record I correspond to the auto-correlation functions of Figure 2).

The best fits of the filters-corrected Lorentzian model (8) to the signal PSD of a record I for each sampling rate are also present in Figure 3. The fitting range was chosen to be $f \in [1, 25]$ kHz. The PSD values below 1 kHz strongly fluctuate and are different in the data records, I, II, III; thus, they are neglected in the fitting procedure (see Section *Discussion*).



A



B

Fig. 3 The signal PSD of the ion current fluctuations sampled at 50 kHz rate (A) and at 250 kHz rate (B). The thick solid line is the fit by the filters-corrected Lorentzian model, Eq. (8); the dashed line is the same Lorentzian model but corrected for the Bessel filter only, i.e., without the sampling correction. The dotted line in (B) is the fit by the pure Lorentzian filters-incorrected model (3). More traditional double-logarithmic scale PSD plots are shown in ESI.

Only the upper bound of the correlation time may be determined as it was indicated above; τ_c was set to zero for the plots on Figure 3. The Lorentzian factor, a , obtained by the fitting has the values of $2.6 \text{ pA}^2/\text{kHz}$ and $2.7 \text{ pA}^2/\text{kHz}$ for the data sampled at 50 kHz rate and at 250 kHz rate, respectively. The same order of dispersion in a is observed between the different data records (I,II,III) within the same sampling rate measurements. To demonstrate the effect of the sampling correction, we also plot $G_m(f)$ without the $|H_s(2\pi f)|^2$ factor (dashed lines in Figure 3, panels A and B). The fit of the pure Lorentzian, filters-incorrected PSD profile to the signal PSD is presented in Figure 3(B); the parameters are $a = 3.5 \text{ pA}^2/\text{kHz}$

and $\tau_c = 0.03$ ms.

Then, we averaged a over the data records (I,II,III) and estimated the error as the maximum between the fitting errors and the averaging error. The concentration dependence of the obtained Lorentzian factor, a , is quite smooth (see Figure 4A as an example).

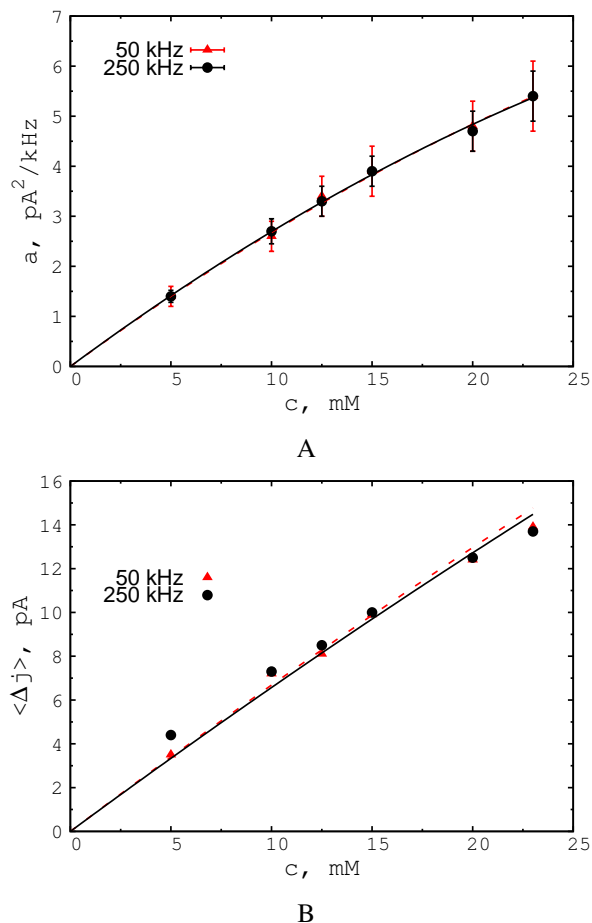


Fig. 4 The meropenem concentration dependence (data set 3, see Tab.1) of (A) the Lorentzian factor, a , and (B) the average ion current shift, $\langle \Delta j \rangle$. The curves are the fits with the parameters presented in Table (2). The red triangles and dashed curves correspond to the 50 kHz sampled data; the black circles and solid lines correspond to 250 kHz samples data.

The average ion current shift, $\langle \Delta j \rangle$, averaged also over the data records (I,II,III), is also fairly smooth vs concentration (see Figure 4B as an example), permitting the use of *Method 3* outlined in Section *Theory* for the determination of the parameters. The fitting parameters, corresponding to the data on Figure 4, are presented in Table 2. The related parameters of blockage kinetics are collected in Table 3.

The kinetic parameters of the meropenem-induced channel blockage determined by *Method 3* for all the sets of data are

Table 2 The fitting parameters for ion-current fluctuations (data set 3) due to channel blockages, determined by using *Method 3* (see Section *Theory*, for details). The absolute error estimates are given in round brackets.

f_s , kHz	b_a	r	b_j
50	0.293 (0.019)	0.0029 (0.0011)	0.688 (0.015)
250	0.297 (0.013)	0.0031 (0.0008)	0.678 (0.020)

Table 3 Kinetic parameters of ion-current fluctuations (data set 3) due to channel blockages, determined by using *Method 3* (see Section *Theory*, for details). The absolute error estimates are given in round brackets.

f_s , kHz	Δj , pA	k_{off} 1/ms	k_{on} 1/(ms M)
50	80 (30)	700 (250)	2030 (140)
250	72 (16)	660 (150)	2060 (140)

presented in Table 4. Sets 1 and 2 do not allow one to de-

Table 4 OpmF/meropenem kinetic parameters of ion-current fluctuations due to channel blockages, determined by using *Method 3* (see Section *Theory*, for details). The data sampled at 50 kHz were used. The absolute error estimates are given in round brackets.

set	Δj , pA	k_{off} 1/ms	k_{on} 1/(ms M)
1	NA	NA	800 (500)
2	NA	NA	800 (400)
3	80 (30)	700 (250)	2030 (140)
4	140 (70)	1200 (600)	1500 (100)
5	80 (20)	750 (200)	2030 (140)

termine the parameters by *Method 3*, being the uncertainty of the fitting parameters near 100%. However, from the sets 3 to 5 one concludes that the Δj value is equal (within the uncertainty error) to 1/3 of the ion current through the open trimer channel. The latter suggests that the monomer channel is completely blocked by an antibiotic molecule. By using the above assumption, we applied *Method 4* to re-analyze all the data sets. The results are presented in Table 5. In addition, we calculated the equilibrium binding constant according to the definition, $K = k_{\text{on}}/k_{\text{off}}$, by using the obtained rate constants (column 5 of Table 5) as well as by using the conductance probe method⁵, K_{cp} (column 6 of Table 5). The available value of K_{cp} are in good accordance with those obtained by our approach.

5 Discussion

For the fast channel-blocking events, the correlation time of the original ion-current fluctuations, τ_c , is less than the inverse cutoff frequency of the subsequent low-pass filter. The observable signal does not permit time resolved blockage events to

Table 5 OpmF/meropenem kinetic parameters of ion-current fluctuations due to channel blockages, determined by using *Method 4* (see Section *Theory*, for details). The data sampled at 50 kHz were used. The absolute error estimates are in round brackets. The equilibrium binding constants calculated within the presented method and those obtained by using the conductance probe method⁵ are presented in columns 5 and 6, respectively.

set	Δj , pA	k_{off} 1/ms	k_{on} , 1/(ms M)	K , 1/M	K_{cp} , 1/M
1	73 (2)	370 (100)	800 (400)	2.2	NA
2	70 (2)	340 (80)	800 (400)	2.3	NA
3	66 (2)	600 (40)	2030 (120)	3.4	3.6
4	66 (2)	540 (40)	1430 (110)	2.6	2.1
5	68 (2)	580 (50)	2000 (200)	3.4	3.3

be detected¹⁶, as in the case of meropenem interaction with OpmF seen in Figure 1A. Hence, the kinetic parameters of the channel blocking can not be deduced in the standard way⁷. The ion-current events histogram does not have a clear secondary peak due to the blockages but instead has a tail as seen in Figure 1B, and therefore the current change Δj in the blocked monomer channel also can not be determined directly. Fingerprints of the channel blockages due to the interaction with the antibiotic are observed in the strong asymmetry of the ion-current event histogram as well as in the antibiotic concentration dependence of the average current and of the current fluctuations. The latter two properties are used to quantify the channel blockage kinetics of meropenem in OpmF in the present study.

The observed auto-correlation function, $R(\tau)$, of the ion-current signal presented on Figure 2 looks confusing at the first sight. First, it has a clear non-exponential form (this is particularly evident for the data sampled at 250 kHz rate) and, thus, is not reproducible by the one-binding-site Markovian model of channel blocking. Second, the correlation time estimated as the width of $R(\tau)$ is about 30 μs , i.e., the blockage events would be observable directly, but they are not. Actually, the shape of this auto-correlation function is mainly determined by the low-pass Bessel filter while the magnitude does depend on the antibiotic induced blockages.

Instead of computing the filters correction to $R(\tau)$, we turn to the equivalent Fourier representation and consider the correction to the power spectral density of the signal, which is fairly simple, given by Eq. (8). By fitting the filters-corrected model PSD to the observed data, we find that the correlations time of the blockage process is less than 5 μs . Thus, the shape of the PSD presented in Figure 3 is determined by the transfer functions of the filters in the examined frequency range. The Lorentzian factor, a , determines the magnitude of the PSD.

For the low-pass 4-pole Bessel filter with 10 kHz cutoff frequency used in the current experiment, the sampling correction to the PSD is important for the 50 kHz sampling (Figure

3A), while for the 250 kHz sampling the effect of the correction is negligible (Figure 3B). The Lorentzian factor and the bounds of the correlations time determined by fitting the filters-corrected Lorentzian to the signal PSD are the same within the fitting errors. Thus, by using the current low-pass analogous filter, one may record the current at 50 kHz rate and analyze with the sampling correction taken into account. Alternatively, one may collect the current at 250 kHz rate, being in this case the sampling correction not necessary.

To appreciate the power of our approach, we fitted the signal PSD with a pure uncorrected Lorentzian (see Figure 3B). It becomes clear that the shape of the Lorentzian is not compatible with the signal PSD, especially for the high frequency tail which decays as $1/f^2$ for the Lorentzian compared to $1/f^8$ for the Bessel filter, as it was discussed in *Electronic Supplementary Information*. While the Lorentzian factor a obtained in such fitting may be quite close (within 30%) to the one obtained by using the filter corrections, the correlation time $\tau_c = 0.03$ ms is completely incorrect. It is close to the width of the autocorrelation function discussed above and characterize the filter rather than the channel blockages due to the antibiotic.

At a lower frequency range, the signal PSD exhibits strong fluctuations between the data records (see Figure 3). These very slow current fluctuations may come from the infrequent partial channel gating or uncontrollable changes in the external conditions (e.g., temperature). We excluded range $f \in [0 : 1]$ kHz from the fitting procedure and, thus, got rid of slow uncontrollable processes. This is a clear advantage of using the Fourier space analysis instead of the real space analysis (auto-correlation function, event counting), for which it is difficult to separate these slow processes from the signal.

In *Method 3* discussed in Section *Theory*, one fits the antibiotic concentration dependence of the Lorentzian factor, $a(c)$, and of the average current shift, $\langle \Delta j \rangle (c)$, with quadratic functions. This provides 3 fitting parameters, b_a, b_j, r from which one may extract the blockage kinetic parameters, $k_{\text{on}}, k_{\text{off}}$, and also Δj . The $\langle \Delta j \rangle$ values, however, are very sensitive to the slow changes of the external conditions (like temperature). For example, from the data presented in Figure 4b, the second-order coefficient, r , may not be extracted due to large fitting errors. In contrast, from the $a(c)$ data of Figure 4a, b_a and r values can be extracted and, by using, $\langle \Delta j \rangle (c)$ b_j is estimated. Still, the uncertainty in r is quite large, about 30% (see Table 2) but the kinetic parameters and the $\langle \Delta j \rangle$ value can be determined (Table 3). The parameters extracted from the analysis of the ion current sampled at 50 kHz and of that sampled at 250 kHz coincide within the estimated error. The corresponding residence time, $\tau_{\text{res}} = 1/k_{\text{off}} = 0.0015 \pm 0.0004$ ms, is in accordance with the correlation-time upper limits determined directly by the fitting the PSD to a filters-corrected Lorentzian.

The obtained reduction of the average ion current through

a single blocked state, Δj , should be compared to its maximal possible value (complete blocking of the current) determined as 1/3 of the average current without antibiotic, $j_0 = 66 \pm 1$ pA. Therefore, a monomer channel is completely blocked by the antibiotic.

The results of the analysis by *Method 3* of all the available data sets (Table 4) indicate that only in two cases (data sets 3 and 5) the kinetic parameters are obtained with a reasonable accuracy. In one case (data set 4) the accuracy of k_{off} and Δj is roughly 50%. In the remaining two cases, only k_{on} can be estimated with an accuracy worse than 50%. In the more recent experiments 3-5, we took special care on the temperature control (see Experiment section) and have considered a wider range of meropenem concentrations (Table 1). In the earlier measurements 1-2, the control of the external conditions was not so good and fewer antibiotic concentrations were considered, and this is the reason of the failure of *Method 3* in those cases.

From the data sets 3 and 5, where the uncertainty of the extracted parameters is small, one concludes that meropenem completely blocks ion current once it is in the monomer channel, i.e., Δj may be estimated as 1/3 of the the average current without antibiotic. By using the latter assumption, we re-analyzed all the data sets with *Method 4*. The obtained kinetic parameters (Table 5) coincide within the uncertainty range with those derived by *Method 3*. The uncertainty for the parameters obtained by *Method 4* is much smaller and also the values for all the measurements are available.

Table 5 also reveals two groups of data. The first one (sets 1-2) gives $k_{\text{on}} \sim 800 \text{ ms}^{-1} \text{M}^{-1}$ and $k_{\text{off}} \sim 350 \text{ ms}^{-1}$. The second one, (sets 3-5) gives $k_{\text{on}} \sim 2000 \text{ ms}^{-1} \text{M}^{-1}$ and $k_{\text{off}} \sim 550 \text{ ms}^{-1}$. The reason of this grouping is not quite clear. It may be due to pore to pore variation, changes in external conditions like temperature (this could likely be eliminated by looking at the conductance which is almost the same over different pores) or due to any other experimental uncertainty. Further analysis is ongoing.

The range of the antibiotic concentrations the method may be applied to is limited from above by the condition of at most one substrate molecule in the channel at a time, i.e., $ck_{\text{on}}/k_{\text{off}} \ll 1$. On the other hand, the ion-current shift, $\langle \Delta j \rangle$, due to the channel blockages by the antibiotic should be measurable, i.e. be larger than some instrumental accuracy δj . As $\langle \Delta j \rangle$ is proportional to c at small concentrations, from Eq.(6), one may write down the lower-bound condition for the concentrations, $N_c \Delta j c k_{\text{on}} / k_{\text{off}} > \delta j$. Finally, the practical range of the antibiotic concentrations to be used in the measurements read,

$$\frac{\delta j}{N_c \Delta j} \frac{1}{K} < c \ll \frac{1}{K}, \quad (20)$$

where K is the equilibrium constant for the antibiotic-channel

interaction. Thus, the suitable range of concentrations depends both on the channel/substrate interaction properties and on the instrumental accuracy.

6 Conclusion

The report here shows that a careful analysis by the modified power spectral density method, taking into account the sampling and the filter effects, is able to resolve the residence times of 1 μs , and this is a factor of 100 below the inverse cut-off frequency of the experimental setup. We use interaction of meropenem with OmpF as an example to obtain the kinetic parameters by using the PSD method developed here.

The ability to extract the kinetic parameters by using the corrected analysis method, which are otherwise off limits using the conventional methods, becomes necessary. This is particularly important for molecules like antibiotics translocating through general channels, where we expect weak interactions due to the lack of specificity. Apart meropenem, there are other examples where an increased noise in ion current trace does not provide well resolved events. In such cases, the rate constants cannot be obtained because of limited temporal resolution hence the analysis method developed here could be used successfully.

Additionally, a future application of the method will be in combination with Kinetic Monte Carlo simulations²³ to scout possible free energy profiles attributable to events extracted from electrophysiology experiments by the analysis protocols here described.

7 Acknowledgment

The research leading to these results was conducted as part of the Translocation consortium (www.translocation.com) and has received support from the Innovative Medicines Initiatives Joint Undertaking under Grant Agreement nr.115525, resources which are composed of financial contribution from the European Union's seventh framework programme (FP7/2007-2013) and EFPIA companies in kind contribution.

References

- 1 H. Nikaido, *Microbiol. Mol. Biol. Rev.*, 2003, **67**, 593–656.
- 2 J.-M. Pagès, C. E. James and M. Winterhalter, *Nat. Rev. Microbiol.*, 2008, **6**, 893–903.
- 3 L. Fernández and R. E. W. Hancock, *Clin. Microbiol. Rev.*, 2012, **25**, 661–81.
- 4 H. Nikaido, *Science*, 1994, **264**, 382–388.
- 5 R. Benz, A. Schmid and G. H. Vos-Scheperkeuter, *J. Membr. Biol.*, 1987, **100**, 21–29.
- 6 A. H. Delcour, *Annu. Rev. Microbiol.*, 2013, **67**, 179–97.
- 7 E. M. Nestorovich, C. Danelon, M. Winterhalter and S. M. Bezrukov, *Proc. Natl. Acad. Sci. U. S. A.*, 2002, **99**, 9789–94.

- 1
2
3 8 P. R. Singh, I. Bárcena-Uribarri, N. Modi, U. Kleinekathöfer, R. Benz,
4 M. Winterhalter and K. R. Mahendran, *ACS Nano*, 2012, **6**, 10699–707.
5 9 H. Bajaj, Q.-T. Tran, K. R. Mahendran, C. Nasrallah, J.-P. Colletier,
6 A. Davin-Regli, J.-M. Bolla, J.-M. Pagès and M. Winterhalter, *Biochem-*
7 *istry*, 2012, **51**, 10244–9.
8 10 R. Benz, A. Schmid, T. Nakae and G. H. Vos-Scheperkeuter, *J. Bacteriol.*,
1986, **165**, 978–986.
9 11 S. Nekolla, C. Andersen and R. Benz, *Biophys. J.*, 1994, **66**, 1388–97.
10 12 C. Hilty and M. Winterhalter, *Phys. Rev. Lett.*, 2001, **86**, 5624–5627.
11 13 L. Kullman, M. Winterhalter and S. M. Bezrukov, *Biophys. J.*, 2002, **82**,
12 803–12.
13 14 C. Danelon, E. M. Nestorovich, M. Winterhalter, M. Ceccarelli and S. M.
14 Bezrukov, *Biophys. J.*, 2006, **90**, 1617–1627.
15 15 A. Brauser, I. Schroeder, T. Gutschmann, C. Cosentino, A. Moroni, U.-P.
16 Hansen and M. Winterhalter, *J. Gen. Physiol.*, 2012, **140**, 69–82.
17 16 E. Hajjar, K. R. Mahendran, A. Kumar, A. Bessonov, M. Petrescu,
18 H. Weingart, P. Ruggerone, M. Winterhalter and M. Ceccarelli, *Biophys.*
19 *J.*, 2010, **98**, 569–575.
20 17 K. R. Mahendran, C. Chimere, T. Mach and M. Winterhalter, *Eur. Bio-*
21 *phys. J.*, 2009, **38**, 1141–5.
22 18 N. Modi, P. R. Singh, K. R. Mahendran, R. Schulz, M. Winterhalter and
23 U. Kleinekathöfer, *J. Phys. Chem. Lett.*, 2011, **2**, 2331–2336.
24 19 E. Hajjar, A. Bessonov, A. Molitor, A. Kumar, K. R. Mahendran, M. Win-
25 terhalter, J.-M. Pagès, P. Ruggerone and M. Ceccarelli, *Biochemistry*,
26 2010, **49**, 6928–35.
27 20 G. Schwarz, C. Danelon and M. Winterhalter, *Biophys. J.*, 2003, **84**,
28 2990–8.
29 21 S. Orfanidis, *Introduction to Signal Processing*, Prentice Hall, Inc., 96th
30 edn, 1995.
31 22 M. Montal and P. Mueller, *Proc. Natl. Acad. Sci.*, 1972, **69**, 3561–3566.
32 23 M. Ceccarelli, A. V. Vargiu and P. Ruggerone, *J. Phys. Condens. Matter*,
33 2012, **24**, 104012.
34
35
36
37
38
39
40
41
42
43
44
45
46
47
48
49
50
51
52
53
54
55
56
57